Influence of the ion mean free path and the role of oxygen in nitriding processes

C. A. Figueroa, E. Ochoa, and F. Alvarez[a)]
Instituto de Física "Gleb Wataghin," Unicamp, 13083-970, Campinas, SP, Brazil

(Received 2 January 2003; accepted 21 May 2003)

In this article we report the mechanism involved in the nitriding process of stainless steel by ion implantation. The importance of the nitrogen ion mean-free path on the stainless steel nitrated layer obtained by using a broad ion source is established. The energy distribution of the nitrogen ions arriving at the substrate is basically determined by the inelastic scattering suffered by the ions on the way to the material surface, i.e., the ion mean-free-path λ. Besides this effect, the ion current density arriving at the sample surface is modified by the dispersion introduced by the collisions of the nitrogen ions with the chamber background molecules. This multiple scattering process is modeled assuming a stochastic phenomenon and its conclusions used to explain experimental results of hardness, diffusion profile, and nitrated layer thickness. A controlled oxygen-background partial pressure is also introduced and its role on the nitrated layer reported. At relatively low ion energies and oxygen partial pressures, both the diffusion zone and nitrated layer thickness are controlled by the ion current density. Indeed, they follow a linear relationship, provided that the composition of the nitrated layer does not change, i.e., the amount of incorporated nitrogen does not modify the original material crystalline phase. © *2003 American Institute of Physics.*
[DOI: 10.1063/1.1591415]

I. INTRODUCTION

In the last two decades a considerable amount of work has been devoted to study the mechanism involved in the stainless steel nitriding process by ion implantation.[1–4] Due to the complexity of the problem, however, many questions remain unresolved. It would appear that a part of the process is fairly well understood: the nitrogen diffusion deeper in the material bulk after implantation. On the other hand, variables such as chamber pressure, plasma structure, surface mechanism, and gas composition as well as its influence on the nitrated layer are not completely understood. Indeed, we believe that better understanding and control of some of those deposition variables is mandatory to improve the material surface properties. Specifically, adsorption and desorption gases in the chamber, chemical and physical sputtering, nitrogen concentration, and thickness (and composition) of the implanted zone (IZ) are very important parameters to control so as to improve the subsequent nitrogen diffusion deeper in the material bulk. The chamber residual gas is usually air, inducing the formation of a potential barrier on the material surface due to adsorbed oxygen. Indeed, as already reported, this barrier diminishes the nitrogen concentration in the implanted region, jeopardizing its bulk diffusion.[5,6] To overcome this problem, hydrogen is added in adequate amounts into the chamber to clean the surfaces by chemical etching. In fact, chemical and physical sputtering are fundamental to eliminate the potential barrier created by oxygen.[7–9] Physical sputtering by heavy ions is normally used as precleaning treatment or, sometimes, simultaneously during the nitriding process. The presence of heavy argon ions bombarding the material helps to remove oxides and contaminating compounds formed on the implanted region.[10–12]

In spite of the enormous advance in the understanding of the nitriding processes, the physical-chemical characteristics of the plasma-surface interaction at variable oxygen partial pressure have not been studied enough. Moreover, besides the presence of oxygen, we found that the total pressure of the chamber must be considered in the nitriding process. This is an important conclusion for industrial applications, since the total chamber pressure during plasma discharge limits the final energy of the ions impinging the sample.[13] Generally, the thickness and nitrogen concentration of the diffusion zone (DZ) are correlated with the ion energy, current density, and oxygen partial pressure. However, the challenge is how to optimize these parameters in order to increase the concentration of nitrogen in the DZ of the sample.

Many of the difficulties found in the study of the DZ stems from the impossibility of independently controlling several parameters involved in nitriding industrial processes. In order to overcome this difficulty, in this article we study the influence of the total pressure and oxygen partial pressure on nitriding using a beam implantation gun (Kaufman cell). In this type of gun, the ion energy, current density, and ion species bombarding the material are independently controlled. As remarked above, in industrial pulsed plasma machines, the ion energy is basically determined by the inelastic scattering suffered by the ions on the way to the material's surface, i.e., the ion mean-free-path λ, basically determined by the chamber pressure.[13] Moreover, considering that the chamber pressure can be used to vary the mean-free path, the use of a Kaufman cell brings more advantages. Indeed, the use of an ion gun expands the nitriding studies from mean-

a)Author to whom correspondence should be addressed; electronic mail: alvarez@ifi.unicamp.br

TABLE I. Nitriding experimental conditions used during deposition: Nitrogen pp: 10^{-2} Pa ; nominal ion energy: 0.6 KeV; nominal ion current density: 5.7 (mA/cm^2); deposition temperature: 380± 10 °C; implantation time: 60 min. The varied range of oxygen pp is indicated. The term λ is the ion mean-free path and L/λ, indicates the average number of collisions for an ion traveling a length L.

Hydrogen partial pressure (pp) (Pa)	Oxygen partial pressure (pp) range (Pa)	Total chamber pressure range (pp) (Pa)	L/λ
...	From 10^{-4} to 10^{-2}	From 10^{-2} to 2×10^{-2}	~0.25
8.2×10^{-1}	From 10^{-4} to 10^{-2}	From 8.3×10^{-1} to 8.4×10^{-1}	~16

free path found in industrial installations to those found in high vacuum conditions. Moreover, high vacuum conditions prevent undesirable contamination. Finally, the experimental results obtained in these unique experimental facilities are then compared with a stochastic scattering model determining the average ion energy as a function of the mean-free path.

II. EXPERIMENT

Rectangular samples, 20×10 mm and 1 mm thick, from the same AISI 316 stainless steel source were used for all the studies. The treated samples were mirror polished using standard metallurgical techniques. The nitriding experiments were performed in an ion beam apparatus with a 3-cm-diam dc Kaufman ion source. More detailed descriptions of the implantation system are found elsewhere.[14] The background chamber pressure is $<10^{-4}$ Pa. The gases are introduced in the Kaufman ion source through mass flowmeter controllers and the ion impacts normal to the surface samples. The chamber pressure is monitored using a Varian cold cathode gauge. The absolute pressure values are obtained using the appropriate gas correction factor provided by the manufacturer.[15] The samples studied were implanted at 380 °C on a temperature-controlled substrate holder. The nominal nitrogen current density of the ion beam was 5.7 mA/cm^2 for all experiments. This nominal current is obtained by dividing the beam current of the Kaufman ion source by the geometrical beam area. This current density must be interpreted as the initial one leaving the gun. However, depending on the total pressure in the chamber, i.e., the scattering introduced by background molecules, different current densities are measured at the surface sample. Then, the true current densities arriving at the sample were determined by a Faraday cup.[16,17] Completing the experimental conditions, the nominal ion energy of the beam was fixed at 0.6 KeV. To consider energy losses, an inelastic scattering theoreticall model was developed to evaluate the final ion energy distribution.

Two series of nitriding experiments were performed. (1) For fixed total chamber pressure (at two extreme conditions) the background oxygen partial pressure is varied by feeding the gas from an independent inlet (Table I). (2) For fixed background oxygen partial pressure, the total chamber pressure is varied by bleeding hydrogen into the chamber (Table II). It is stressed that the Kaufman source starts with pure nitrogen gas in such a way as to obtain the adequate nominal ion current (~5.7 mA/cm^2). Thereafter, by flooding the chamber with hydrogen from an independent inlet (i.e., not through the Kaufman cell), the chamber adequate pressure is reached.

The hardness was obtained using a Berkovich diamond tip (NanoTest-300) at depths varying between 50 and 1800 nm and the results analyzed using the Oliver and Pharr method.[18] The indentation was perpendicular to the nitrated surface and the tip load controlled the penetration depth. Piling-up effects were not considered. The cross section of the nitrated layers was revealed by attacking the samples at room temperature with Marble's solution (10 g copper sulfate in 100 ml of 6 M hydrochloric acid) and measured by scanning electron microscopy (SEM / JEOL JMS-5900LV). The nitrated layer thickness was directly measured from the SEM images.

III. RESULTS

A. Effect of the background pressure: The role of oxygen

The number of inelastic collisions determines the ultimate energy and flux of the ions impinging on the substrate. Also, the background chamber pressure determines the mean-free path of the ions arriving at the sample. Assuming that the distance between the Kaufman exit and sample is L the ratio L/λ is the average number of collisions before an ion impinges on the sample. Two very different L/λ ratios (~0.25 and 16) and variable partial pressure of oxygen were used in this study (Table I). As explained in Sec. II, the background chamber pressure was obtained by bleeding hydrogen into the chamber. Figure 1 shows typical curves of hardness profiles versus depth at the two different L/λ stud-

TABLE II. L/λ ratios at different total pressures, controlled by bleeding H_2 in the chamber. Here λ is the ion mean-free path and L/λ indicates the average number of collisions for an ion traveling a length of L. Oxygen pp, 5×10^{-4} Pa; nitrogen pp, 10^{-2} Pa; nominal ion energy: 0.6 KeV; nominal ion current: 5.7 (mA/cm^2); deposition temperature: 380± 10 °C; implantation time: 60 min.

Total pressure (Pa)	L/λ
8.3×10^{-1}	16
4.1×10^{-1}	8.13
1.1×10^{-1}	2.15
6.0×10^{-2}	1.19
3.0×10^{-2}	0.62
1.7×10^{-2}	0.38
1.0×10^{-2}	0.25

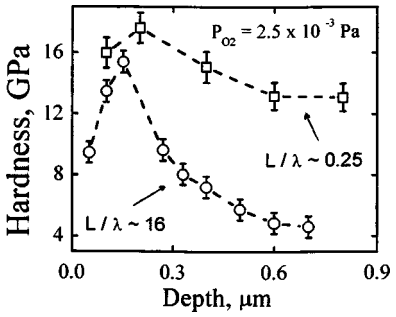

FIG. 1. Hardness vs depth obtained at two extreme conditions of total chamber pressure as a function of L/λ (average number of collisions). The experiments are performed at $P_{02}=2.5\times10^{-3}$ Pa. The lines are a guide for the eyes.

ied. The decreasing of the hardness on increasing L/λ is quite remarkable. Figure 2(a) shows the total nitrogen depth penetration as a function of oxygen partial pressure implanted at two different L/λ. As in the case of hardness, a similar tendency is observed: the nitrogen penetration decreases on increasing L/λ, i.e., number of collisions. We note that, for a higher L/λ ratio, the maximum of the curve slightly shifts to lower oxygen partial pressure. For the hardness measured at 0.4 μm depth, a similar trend is also observed [Fig. 2(b)].

B. Nitrogen implantation: The role of the mean free path, λ

In order to understand the differences described in Sec. A, it is important to explore the nitrogen implantation dependence on total pressure, i.e., as a function of the number of collisions L/λ. The number of collisions is controlled by increasing the partial pressure of the background hydrogen and, simultaneously, maintaining constant oxygen partial pressure (Table II). Figure 3 shows the hardness at two fixed

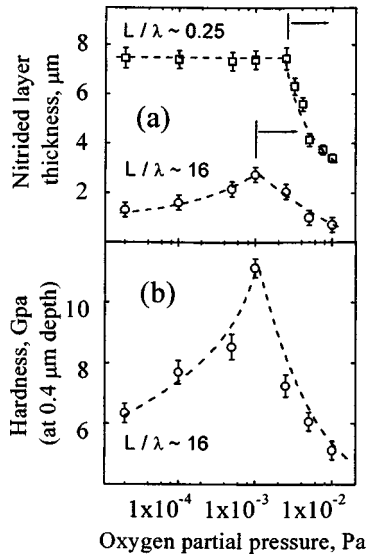

FIG. 2. (a) Nitrided layer thickness (depth penetration) vs oxygen partial pressure obtained at two extreme conditions of L/λ (average number of collisions); (b) hardness (at constant depth) vs oxygen partial pressure ($L/\lambda\sim16$). The lines are a guide for the eyes.

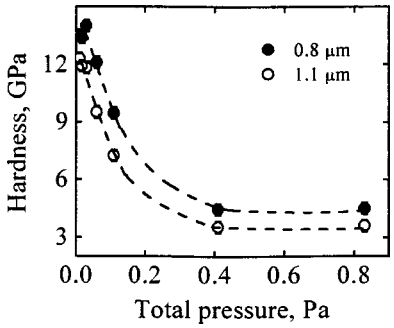

FIG. 3. Hardness vs total chamber pressure at two different depths. The lines are a guide for the eyes.

different depths versus chamber total pressure. The strong decay tendency of the curves is quite visible. As in the case of the hardness, the total thickness of the diffusion zone of these samples follows the same trend as a function of the chamber total pressure (not shown).

IV. DISCUSSION

The phenomena occurring at the material surface during nitration, plasma structure and characteristics of the implanted nitrogen region, are relevant to control the nitrogen diffusion into the bulk. The neutral gases present in the chamber usually interact with the plasma and with the material surface. Depending on the total chamber pressure, inelastic scattering produces ion energy and current density losses, modifying the energy distribution and intensity of the beam. Regarding the ion energy distribution, two tendencies on the final nitrated layer profile are reported in the bibliography: (1) nitrogen profiles independent of ion energy,[19] and (2) nitrogen profiles depending on ion energy.[13,20] In the nitriding process, it is generally accepted that the ion current density is more relevant than the ion energy determining the DZ.[21,22] The chamber gases interacting with the surface play an active role in the nitrogen diffusion mechanism. For instance, oxygen has the characteristic of being easily adsorbed, profoundly changing the physic-chemical properties of the surface.[23] Also, besides the surface process and subsequent diffusion into the bulk, a complex inelastic scattering mechanism of the bombarding species influences the implanted zone (IZ). This zone depends strongly on ion energy and current density, and determines the boundary conditions for nitrogen diffusion. Indeed, the nitrogen concentration in this layer is the chemical potential or activity coefficient (thermodynamically speaking) of the process. Therefore, the retained surface ions fix the chemical potential at the implanted zone, controlling the nitrogen diffusion driving force.

Figure 1 shows the dependence of hardness (for two L/λ conditions) as a function of depth. As observed, the hardness profile is increasing for L/λ ratios going from 16 to 0.25. Figure 2(a) shows the nitrogen total depth penetration for the two studied ratios of L/λ as a function of oxygen partial pressure. The bizarre behavior of the curves was associated with an augment of nitrogen retention for low O_2 pressure. For higher O_2 partial pressure ($>10^{-3}$ Pa), due to the formation of oxidized barriers, the hardness and thickness pen-

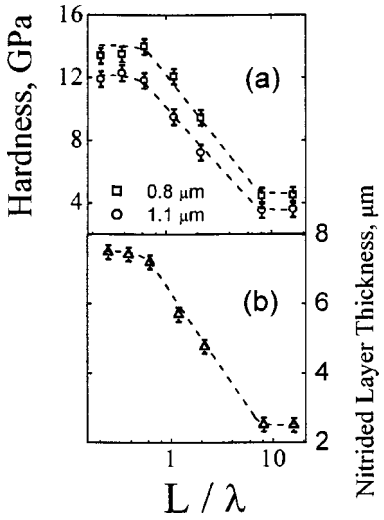

FIG. 4. (a): Hardness vs L/λ at two different depths. (b) Nitrided layer thickness vs L/λ. The lines are a guide for the eyes.

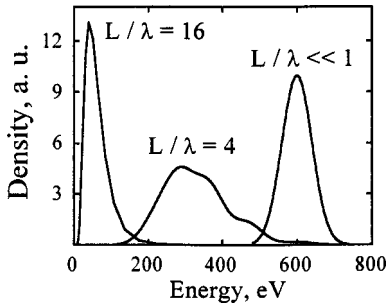

FIG. 5. Ion energy distributions at different L/λ ratios using an inelastic scattering model.

etration diminishes[5,7] As expected, the hardness of the nitrated layer at a fixed depth (0.4 μm) *versus* oxygen partial pressure [Fig. 2(b)] shows the same behavior observed in Fig. 2(a).

Figure 3 shows the strong-decay behavior of hardness versus total chamber pressure at two arbitrarily fixed depths. As remarked above, an increasing chamber pressure decreases the mean-free path of the ions, i.e., an augment of the number of inelastic collisions. Consequently, the ion energy and current density losses diminish the number of implanted nitrogen, explaining why the hardness decreases monotonically as the chamber pressure increases. The mean-free-path λ is estimated by the kinetic theory of gases and the hardness plotted as a function of the L/λ ratio [Fig. 4(a)]. As above, the ion ''fly length'' L is the distance between the Kaufman exit window and the sample. The plot shows a break point ($L/\lambda \sim 0.8$) where the inelastic scattering starts to jeopardize the formation of a good-nitrated layer.

In the attempt to correlate the scattering ion energy losses and the nitrated layer, we discuss a model determining the ion energy distribution arriving at the sample. First, we shall estimate the ion energy distribution arriving at the sample surface for different chamber total pressures. At the working pressures of the experiments, the distance traveled between successive collisions follows an exponential decay curve, i.e., $\sim \exp(-x/\lambda)$. [24] For a $L/\lambda = 1$ ratio, 37% of ions are not expected to collide with other molecules present in the chamber. In other words, there is a 63% chance that an ion traveling λ does hit any other chamber molecule. Therefore, the initial ion energy distribution will change after successive collisions. Assuming N ions, the fraction of particles having suffered k collisions (''success'') after traveling n mean-free path follows a binomial distribution probability

$$c_k = \{n!/[k!(n-k)!]\}\, p^k (1-p)^{n-k}. \tag{1}$$

Here $k \leqslant n$ represents the number of mean-free paths traveled by the particles; $p = 0.63$ is the probability of an individual collision.

A Gaussian initial distribution is a realistic assumption in a Kaufman ion source.[16] In our experimental conditions, typical initial values for σ and E_0 are 40 and ~ 600 eV, respectively. Here σ and E_0 represent the variance and the mean value of a Gaussian distribution. After traveling n mean-free paths there will be $n+1$ distributions, i.e., one distribution for each successful k collision. Figure 5 shows the obtained energy distributions at three different L/λ ratios using this simple model. For small L/λ ratios (few collisions), the final distributions resemble the initial one. On the contrary, large L/λ ratios considerably modify the initial ion energy distribution. The final ion energy distribution is written as

$$F(E) = \sum_{k=0}^{n} c_k f_k(E), \tag{2}$$

where the c_k are given by Eq. (1), i.e., this coefficient represents the probability of obtaining k success (collisions) when n events (n mean-free-path λ traveled by the ion) occurred, and f_k is the density function of a normal distribution of the ions after k success (collisions) given by

$$f_k(E) = [1/(2\pi\sigma^2)^{1/2}] \exp\{-[E-(E_0 r^k)]^2/2\sigma^2, \tag{3}$$

where σ and E_0 are defined above. The factor r is related to the energy loss by individual collision. Assuming frontal collision, $r = (m_{N_2} - m_{H2})^2/(m_{N_2} + m_{H_2})^2 = 0.75$, where m_i ($i = N_2, H_2$) are the molecular mass of the involved particles in the collision. Here, due to the energies involved in the process, this factor is obtained assuming hard sphere collisions.[24]

The ion current density and mean ion energy at different total pressures were experimentally determined by using a Faraday cup[16] and calculated by the above model, respectively, at surface sample (Table III). Figure 6 shows the ion energy and current density versus L/λ and the same trends as Fig. 4 are observed.

As discussed above, the nitrogen concentration in the implanted zone is another important ingredient determining the final nitrated layer. Using a standard implantation model (TRIM[25]), it is possible to model this region beneath the surface. Tian and Chu measured nitrogen concentration *versus* depth in samples implanted at variable ion energy.[20] These researchers reported different profiles up to ~ 175 nm penetration depths for ion energies varying between 8 and 25 KeV agreeing very well with the TRIM calculus. These re-

TABLE III. Final mean ion energy, ion current density, and implanted zone thickness at variable total pressure: background pressure: $<10^{-4}$ Pa; oxygen partial pressure (pp): 5×10^{-4} Pa; nitrogen pp: 10^{-2} Pa; nominal ion energy: 0.6 KeV; nominal ion current density 5.7 (mA/cm^2); deposition temperature: 380 ± 10 °C; implantation time: 60 min.

Total pressure (Pa)	Mean ion energy (calculated) (eV)	Ion current density (mA cm^{-2})	IZ thickness (TRIM) nm
8.3×10^{-1}	50	0.31	4
4.1×10^{-1}	174	0.32	8.4
1.1×10^{-1}	441	0.76	13.1
6×10^{-2}	516	0.97	15.2
3×10^{-2}	556	1.19	16.6
1.7×10^{-2}	572	1.23	17.3
1×10^{-2}	584	1.23	17.6

searchers also reported that at a deeper depth, the implanted profiles all merge together. Indeed, in our implanted samples the hardness is constant at deeper distances than ~200 nm, a result consistent with a constant nitrogen concentration.[7] These experimental results together with the theoretical model suggest that the energy of the ion determines the thickness of the IZ (see Table III). On the other hand, the lack of changes of the DZ indicates that there is no appreciable increase of the chemical potential, a key parameter determining the driving diffusion force.

The effective nitrogen diffusion into the bulk is related to nitrogen concentration in the IZ, a parameter intimately associated with the ion current density. If this is so, one can postulate a linear relationship between the nitrided layer thickness d_N and the ion current density I_{ion}

$$d_N = c \times I_{ion}, \tag{4}$$

where c is a constant. Indeed, Fig. 7 is clearly in agreement with this postulate. It is important to remark, however, that this relationship is valid provided that the nitrided phase γ' maintains the crystalline fcc structure. The inset shows the hardness normalized to ion density versus ion energy. The almost constant value suggests that the arriving energy is not predominantly important on the final hardness of the material. The regime of low oxygen partial pressure used in the experiments at variable total pressure, and the utilization of hydrogen to regulate total pressure, reduce the formation of an oxidized surface potential barrier. Therefore, the ion current density is indeed the important parameter to increase the nitrogen concentration in the material bulk. In fact, the use of high ion energy ions is mandatory to break up the oxidized layer formed in conditions of poor vacuum nitrogen implantation.

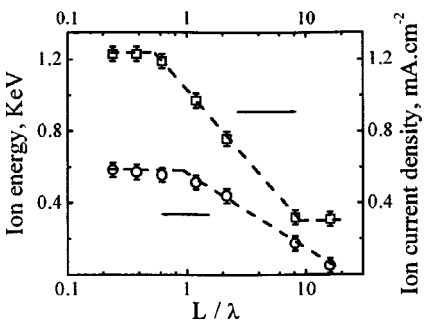

FIG. 6. Mean ion energy and ion current density at the sample surface vs L/λ. The lines are a guide for the eyes.

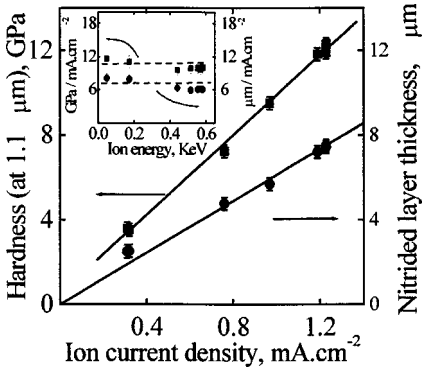

FIG. 7. Linear dependence of the hardness (at constant depth) and nitrided layer thickness vs ion current density (at the surface sample). Inset: hardness and thickness normalized to ion density vs ion energy in (GPa/mA cm^{-2}) and (μm/mA cm^{-2}), respectively.

Finally, Fig. 2 shows that adding enough oxygen in the chamber will diminish the amount of nitrogen in the IZ. This can be understood as due to the formation of an oxidized surface potential barrier. Moreover, increasing the chamber pressure also increases the inelastic scattering, reducing the ion current density. This effect reduces the erosion by sputtering and consequently shifting the maximum of the nitrated layer thickness for different ion density currents.

V. CONCLUSIONS

The effects of the nitrogen ion mean-free paths and oxygen partial pressure on the hardness properties of implanted SS 316 are reported. Chamber total pressures similar to those used in industrial systems increase ion scattering, jeopardizing efficient nitrogen incorporation in the material. A stochastic scattering model is proposed to estimate the ion energy distribution arriving at the substrate, which allows explaining the experimental data. Nitriding experiments at constant oxygen partial pressure ($\sim5.10^{-4}$ Pa) and different nitrogen mean-free path, allows one to draw the following conclusions: (a) the thickness and hardness of the diffusion zone are independent of ion energy; and (b) the thickness and hardness are also directly proportional to ion current density, provided that the nitrided phase remains invariant. Finally, for higher pressures, adsorbed oxygen on the surface forms a potential barrier for the ions. In this situation, higher ion energies could help to improve the nitrogen penetration into the material by removing the oxidized layer.

ACKNOWLEDGMENTS

This work is part of the Ph.D. thesis of C.A.F. The authors are indebted to D. Ugarte, M. Bica, and M. I. Romero for helping with some measurements and to D. Wisnivesky for interesting discussions. The work was partially sponsored by FAPESP, project No. 97/12069-0. C.A.F. is a FAPESP fellow. E.O. and F.A. are CNPq fellows.

[1] A. H. Deutchman, R. J. Partyka, and C. Lewis, Conference Proceedings of the ASM - second International Conference Cincinnati, Ohio, 18–20 September, 1989, edited by T. Spalvins and W. L. Kovacs (ASM Int., Metals Park, OH, 1989), p. 29.
[2] Z. L. Zhang and T. Bell, Surf. Eng. **1**, 131 (1985).
[3] F. El-Hossary, F. Mohammed, A. Hendry, D. F. Fabian, and Z. Szaszne-Csih, Surf. Eng. **4**, 150 (1988).
[4] A. Ramchandani and J. K. Dennis, Heat Treat. Met. **2**, 34 (1988).
[5] W. Möller, S. Parascandola, O. Kruse, R. Günzel, and E. Richter, Surf. Coat. Technol. **116–119**, 1 (1999).
[6] W. Möller, S. Parascandola, T. Telbizova, R. Günzel, and E. Richter, Surf. Coat. Technol. **136**, 73 (2001).
[7] C. A. Figueroa, D. Wisnivesky, and F. Alvarez, J. Appl. Phys. **92**, 764 (2002).
[8] S. Kumar, M. J. Baldwin, M. P. Fewell, S. C. Haydon, K. T. Short, G. A. Collins, and J. Tendys, Surf. Coat. Technol. **123**, 29 (2000).
[9] J. M. Priest, M. J. Baldwin, and M. P. Fewell, Surf. Coat. Technol. **145**, 152 (2001).
[10] D. L. Williamson, J. A. Davis, and P. J. Wilbur, Surf. Coat. Technol. **103,104**, 178 (1998).
[11] A. Leyland, D. B. Lewis, P. R. Stevenon, and A. Mathews, Surf. Coat. Technol. **62**, 608 (1993).
[12] A. Saker, Ch. Leroy, H. Michel, and C. Frantz, Mater. Sci. Eng., A **140**, 702 (1991).
[13] R. Wei, Surf. Coat. Technol. **83**, 218 (1996).
[14] P. Hammer, N. M. Victoria, and F. Alvarez, J. Vac. Sci. Technol. A **16**, 2941 (1998).
[15] Multi-Gauge Controller, Manual 6999-08-091, Revision U, December 1998. Varian Vacuum Tech., Lexington, MA.
[16] H. Ch. Paulini, and U. Littmark, Nucl. Instrum. Methods Phys. Res. B **58**, 260 (1991).
[17] D. Van Vechten, G. K. Hubler, and E. P. Donovan, Vacuum **36**, 841 (1986).
[18] W. C. Oliver and G. M. Pharr, J. Mater. Res. **7**, 1564 (1992).
[19] C. A. Figueroa, D. Wisnivesky, P. Hammer, R. G. Lacerda, R. Droppa, Jr., F. C. Marques, and F. Alvarez, Surf. Coat. Technol. **146,147**, 405 (2001).
[20] X. Tian and P. K. Chu, J. Vac. Sci. Technol. A **19**, 1008 (2001).
[21] S. Leigh, M. Samandi, G. A. Collins, K. T. Short, P. Martin, and L. Wielunski, Surf. Coat. Technol. **85**, 37 (1996).
[22] V. A. Kukareko and A. V. Byeli, Surf. Coat. Technol. **127**, 174 (2000).
[23] S. Parascandola, O. Krase, and W. Möller, Appl. Phys. Lett. **75**, 1851 (1999).
[24] B. Chapman, *Glow Discharge Processes* (Wiley-Interscience, New York, 1980).
[25] J. P. B. Biersack and G. L. Haggmark, the simulation used the TRIM software, Nucl. Instrum. Methods **174**, 257 (1980).